Available online at https://rjas.rsu.ac.th
Formerly Rangsit Journal of Arts and Sciences (RJAS)

Journal of Current Science and Technology, July-December 2020 JCST Vol.10 No.2, pp. 165-181

ISSN 2630-0656 (Online)

Eliminating the static errors of state variables by using real-time cascaded flatness-based control for induction motors

Pham Tam Thanh[1*], Xuan-Kien Dang[2], and Le Anh-Hoang Ho[3]

[1]Vietnam Maritime University, Hai Phong, Vietnam
[2]HoChiMinh City University of Transport, Ho Chi Minh City, Vietnam
[3]Van Hien University, District 3, Ho Chi Minh City, Vietnam

*Corresponding author; Email: phamtamthanh@vimaru.edu.vn

Received 10 May 2020; Revised 2 June 2020; Accepted 24 June 2020
Published online 22 July 2020

Abstract

Induction Motor (IM) can be found in many industrial applications such as precision machining and automation processes, especially robotics. In this paper, firstly, we investigate the problem of nonlinear discrete-time flatness-based controller design for IM. Secondly, we propose a new control strategy named cascaded flatness-based control (CFBC) by considering the nonlinear characteristics of IM in order to eliminate the static errors of state variables. Simulation is shown to demonstrate the benefits of the proposed CFBC and the performance evaluation is given by experimental results.

Keywords: *flatness-based control, induction motor, nonlinear system, real-time control*

Nomenclature

Symbol	Description	Symbol	Description
$\mathbf{u}_s$, $\mathbf{i}_s$	Vector of stator voltage, vector of stator current	$\omega, \omega_s, \omega_r$	Mechanical rotor velocity, Stator circuit velocity, Rotor circuit velocity
$\mathbf{i}_s^f$, $\mathbf{i}_s^s$	Vector of stator current $\mathbf{i}_s$: Field synchronous or rotor flux orientated coordinate system dq, stator-fixed coordinate system $\alpha\beta$	$\boldsymbol{\psi}_p$, ψ_p	Vector of pole, pole flux
		$\boldsymbol{\psi}_s$, $\boldsymbol{\psi}_r$	Vector of stator flux, vector of rotor flux
		$\psi_{rd}, \psi_{rq}, \psi_{sd}, \psi_{sq}$,	dq components of the rotor, stator flux
i_{su}, i_{sv}, i_{sw}	Stator current of phases u, v, w	$\psi'_{rd}, \psi'_{rq}, \psi'_{r\alpha}, \psi'_{r\beta}$,	Components of $\boldsymbol{\psi}'_r$, $\boldsymbol{\psi}'_s$
i_{sd},i_{sq}	dq components of the stator current	υ, υ_s, υ_u	Rotor angle, angle of flux orientated coordinate system, angle phase of vector voltage $\mathbf{u}_s$
$i_{s\alpha}$,$i_{s\beta}$	$\alpha\beta$ components of the stator current	J	Torque of inertia
m_W, m_M	Load torque, motor torque	L_m, L_r, L_s	Mutual, rotor, stator inductance
$\mathbf{u}_s^f$, $\mathbf{u}_s^s$	Vector of stator voltage $\mathbf{u}_s$: Field synchronous or rotor flux orientated coordinate system dq, stator-fixed coordinate system $\alpha\beta$	$L_{\sigma r}$, $L_{\sigma s}$	Rotor-side, stator-side leakage inductance
		L_{sd}, L_{sq}	d axis, q axis inductance
		R_r, R_s	Rotor, stator resistance
		T,f	Sampling period, Sampling frequency
u_{sd}, u_{sq}	dq components of the stator voltage	T_r,T_s	Rotor, stator time constant
$u_{s\alpha}$,$u_{s\beta}$	$\alpha\beta$ components of the stator voltage	T_{sd},T_{sq}	d axis, q axis time constant
		z_p	Number of pole pairs
s	Slip	σ	Total leakage factor

1. Introduction

Induction Motor (IM) can be found in many industrial applications such as marine control systems, precision machining and automation processes, marine systems, especially robotics. Due to the advantages of superior power density, highly effectiveness with high speed and accuracy, the problem of control design for IM is not only in relation to low cost and high reliability but also the efficient use of energy (Beaty & Kirtley, 1998; Wang, Zhong, Yang, & Mu, 2010). However, there remain some interesting questions related to how to design a controller so that the static errors of the system state variables are minimized. Noticeably, the nonlinear characteristics of the IM are taken into account in the process of control.

Over the past few decades, the concept of differentially flat systems was first introduced by Fliess, Lévine, Martin, & Rouchon, 1992. The system is considered to be flat if the set of outputs can be found such that all states and inputs can be determined from these outputs without integration. The main purpose of the flatness-based control (FBC) method is first to design an open-loop nominal control corresponding to the predicted trajectory of the flat output. Then, a feedback control law is applied to stabilize the real trajectory around the predicted trajectory of the flat output. The FBC has been recognized as a promising method to deal with nonlinear systems (see, e.g., Levine, 2009 and references therein). To minimize the copper loss at all operating points of the Permanent Magnet Synchronous Motor (PMSM), a hierarchical FBC scheme was developed in Delaleau & Stankovic, 2004. However, The FBC needs not only high quality of control but also robustness under the effect of nonlinearity of the IM. Therefore, normal FBC method does not seem reliable enough.

Considering the nonlinearity of IM, there have been usually several methods used to transform a nonlinear system into a linear system so that the system can apply the approach of linear control. In Dannehl and Fuchs, 2006, a nonlinear differential flatness-based control was proposed to the induction machine fed by a voltage source converter in which the flatness-based control was used for the inner current loop as well as the outer flux and speed loops. Based on the combination of the natural energy dissipation properties of the permanent magnet stepper motor system with its differential flatness property, a nonlinear feedback controller was proposed in Sira-Ramirez, 2000. Another approach for drive systems with elastically coupled loads was reported by Thomsen and Fuchs, 2010. To be clear, fuzzy logic has got a great development and lots of important results in order to deal with problems of uncertainty and disturbance of nonlinear system in literatures (Dang, Guan, Tran, & Li, 2011; Do & Dang, 2018; Dang, Ho, & Do, 2018; Do & Dang, 2019). By using fuzzy logic technique to eliminate the effect of the time-varying nonlinearities of an induction motor, a fuzzy differential FBC was developed by Fan and Zhang, 2011a and 2011b. In Houari, Renaudineau, Martin, Pierfederici, and Meibody-Tabar, 2012, a new differential FBC method was presented for a three-phase inverter with an LC filter. Recently, quasi-continuous implementation of structural nonlinear controller based on direct-decoupling for PMSM was presented by our previous work (Thanh & Quang, 2013) and provided the FBC for the PMSM which stimulates the stator current trajectory based on the continuous-time state model of the motor. It should be noted that in the aforementioned papers, the problem of nonlinear FBC has not been fully investigated and the minimization problem of the static errors of state variables has not received important attention.

Based on the discussion aforementioned, the motivation of this paper is to eliminate the static errors of state variables by using a proposed cascaded flatness-based control scheme solving the problems here are: 1) to investigate the problem of nonlinear discrete-time flatness-based controller design for IM, 2) to propose new control strategy named cascaded flatness-based control (CFBC) by considering the nonlinear characteristics of IM in order to suppress the state static errors of IM control system, and 3) to simulate and to do experimental real-time IM hardware model to illustrate the effectiveness of the proposed approach.

The rest of this paper is organized as follows. In Section 2, we introduce a nonlinear discrete-time model of IM. The nonlinear CFBC for IM is presented in Section 3. Section 4 is dedicated to showing the simulation results, analysis, and evaluation of the proposed CFBC model. Next section we deal with the experimental system. Finally, we conclude the paper in Section 6.

2. Discrete-time modeling of induction motors

Consider the current model of IM in the continuous-time form as shown bellow

$$\begin{cases} \dot{x} = f(x) + H(x)u \\ y = g(x) \end{cases} \quad (1)$$

where,

- State vector:

$$x = [x_1 \quad x_2 \quad x_3]^T = [i_{sd} \quad i_{sq} \quad v_s]^T$$

- Input vector:

$$u = [u_1 \quad u_2 \quad u_3]^T = [u_{sd} \quad u_{sq} \quad \omega_s]^T$$

- Output vector:

$$y = [y_1 \quad y_2 \quad y_3]^T = [x_1 \quad x_2 \quad x_3]^T$$

$$f(x) = [-dx_1 + c\psi'_{rd} \quad -dx_2 - cT_r\omega\psi'_{rd} \quad 0]^T \quad (2)$$

$$H(x) = [h_1(x) \quad h_2(x) \quad h_3(x)]^T \quad (3)$$

$$h_1(x) = [a \quad 0 \quad 0]^T$$

$$h_2(x) = [0 \quad a \quad 0]^T$$

$$g(x) = [g_1(x) \quad g_2(x) \quad g_3(x)]^T = [x_1 \quad x_2 \quad x_3]^T \quad (4)$$

and temporary parameters are given by:

$a = 1/(\sigma L_s)$; $b = 1/(\sigma T_s)$; $c = (1-\sigma)/(\sigma T_r)$; $d = b + c$; $e = cT_r\omega$

Note that the functions f(.) and H(.) in equation (1) are inherently nonlinear, the ordinary differential equation (1) cannot be presented exactly. Hence, the exact form of the discrete-time differential equation is difficult to obtain. Therefore, to solve the discrete-time current model of IM, Taylor's series expansion is using as

$$x(k+1) = x(k) + \dot{x}(t)|_{t=kT}T + X(T) \quad (5)$$

where, T is sampling period and $X(T)$ is the higher-order terms of the Taylor's series expansion which can be expressed as follows

$$X(T) = \frac{1}{2!}x^{(2)}(kT)T^2 + \cdots + \frac{1}{n!}x^{(n)}(kT)T^n + \frac{1}{(n+1)!}x^{(n+1)}(\zeta)T^{n+1}, \zeta \in (kT, kT+T) \quad (6)$$

As the sampling period in the advanced electric drive systems is very small, the higher-order terms in equation (6) can therefore be neglected. By substituting (1) into (5), the discrete-time current model of IM is obtained as

$$x(k+1) = x(k) + Tf(x(k) + TH(x(k)u(k) + X(T) \quad (7)$$

$$y(k) = g(x(k))$$

Equation (7) can be rewritten in the form of

$$\begin{bmatrix} x_1(k+1) \\ x_2(k+1 \\ x_3(k+1 \end{bmatrix} = \begin{bmatrix} x_1(k) \\ x_2(k) \\ x_3(k) \end{bmatrix} + \begin{bmatrix} -dx_1(k) + c\psi'_{rd} \\ -dx_2(k) - cT_r\omega\psi'_{rd} \\ 0 \end{bmatrix} T + \begin{bmatrix} a & 0 & -x_2(k) \\ 0 & a & -x_1(k) \\ a & 0 & 1 \end{bmatrix} \begin{bmatrix} u_1(k) \\ u_2(k) \\ u_3(k) \end{bmatrix} T \quad (8)$$

We rewritten as below

$$\begin{bmatrix} x_1(k+1) \\ x_2(k+1 \\ x_3(k+1 \end{bmatrix} = \begin{bmatrix} 1-dT & 0 & 0 \\ 0 & 1-dT & 0 \\ 0 & 0 & 0 \end{bmatrix} \begin{bmatrix} x_1(k) \\ x_2(k) \\ x_3(k) \end{bmatrix} + \begin{bmatrix} aT & 0 & 0 \\ 0 & aT & 0 \\ 0 & 0 & 1 \end{bmatrix} \begin{bmatrix} u_1(k) \\ u_2(k) \\ u_3(k) \end{bmatrix} + \begin{bmatrix} 0 & T & 0 \\ -T & 0 & 0 \\ 0 & 0 & 0 \end{bmatrix} \begin{bmatrix} x_1(k) \\ x_2(k) \\ x_3(k) \end{bmatrix} u_3 + \begin{bmatrix} cT\psi'_{rd}(k) \\ -cTT_r\omega\psi'_{rd}(k) \\ 0 \end{bmatrix} \quad (9)$$

Equation (9) can be written as components

$$\begin{cases} i_{sd}(k+1) = (1-dT)i_{sd}(k) + \omega_s(k)Ti_{sq}(k) \\ \quad +cT\psi'_{rd}(k) + aTu_{sd}(k) \\ i_{sq}(k+1) = (1-dT)i_{sq}(k) - \omega_s(k)Ti_{sd}(k) \\ \quad -cT\omega_r T\psi'_{rd}(k) + aTu_{sq}(k \\ v_s(k+1) = v_s(k) + \omega_s(k)T \end{cases} \quad (10)$$

It is worthy note that the nonlinear characteristics in the current model of IM (9) or (10) are considered in terms of the products of the state variables (current components i_{sd}(k), i_{sq}(k) and input variable $\omega_s(k)$. This nonlinear discrete-time model is used for controller design in the next section.

3. Cascaded flatness-based control for induction model

3.1 Related works

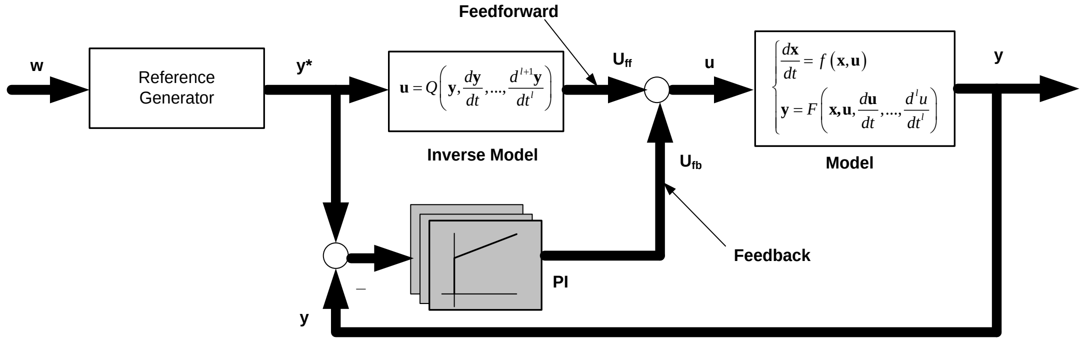

Figure 1 The traditional flatness-based control structure

As mentioned in Fliess et al. 1992 and Fliess et al. 1999, the main property of differential flatness is that the state and input variables can be directly expressed, without integrating any differential equation, in terms of the flat output and a finite number of its derivatives. Therefore, the trajectory of input can be determined from desired trajectory of flat output. The general flatness-based control structure consists of a nominal feedforward controller combined with a feedback stabilizing controller as shown in Figure 1. In this structure, the feedback controller is crucial of importance to compensate the effects of external disturbances and model uncertainties.

To model a predictive control based on flatness theory, Fliess and Marquez, 2000 presented the definition of flatness-based predictive control. Moreover, Maaziz, Siguerdidjane, Boucher, and Dumur, 1999 used the flatness property to achieve reference trajectory of generalized predictive control for the application, and flatness property optimization used to repeatedly for the input of the system (Mahadevan, Agrawal, & Doyle, 2001; Hagenmeyer, & Delaleau, 2003; Hagenmeyer, & Delaleau, 2004; Hagenmeyer, & Delaleau, 2008). Besides that, there are many applications in recent years such as chemical reactors in Graichen, Hagenmeyer, and Zeitz, 2006, mechatronic control system in Henke, Rue, Neumann, Zeitz, and Sawodny, 2014, and Noda, Zeitz, Sawodny, and Terashima, 2011, hydraulic control in Broocker and Lemmen, 2001, permanent magnet synchronous machines in Faustner, Kemmetmüller, and Kugi, 2015, and Faustner, Kemmetmüller, and Kugi, 2016. However, FBC need not only high quality of control but also robustness under the effect of nonlinearity and uncertainty of models. Therefore, FBC method does not seem reliable enough.

3.2 Proposed cascaded flatness-based control

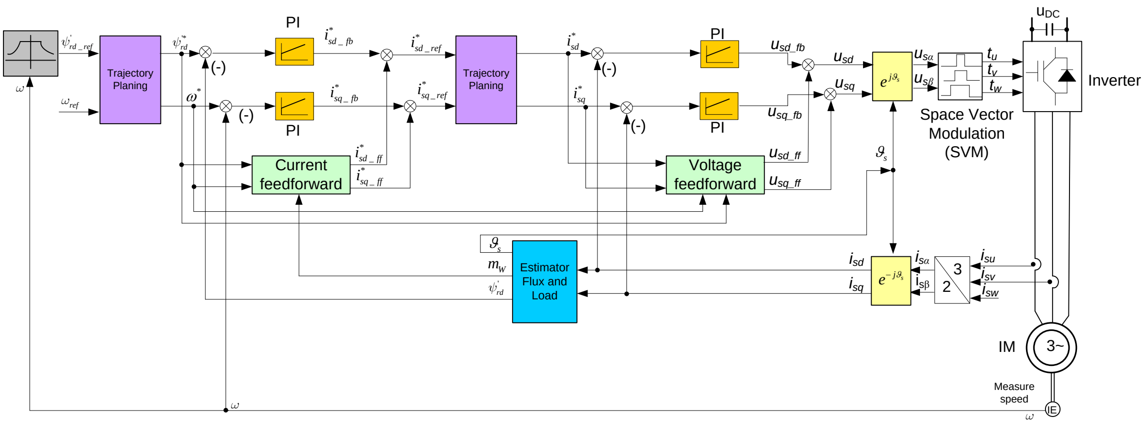

Figure 2 Cascade control structure of flatness-based control of IM

To eliminate the static errors of state variables system state static errors and to consider the nonlinear characteristics of IM, a cascade flatness-based control structure is proposed in Figure 2. As shown in Figure 2, the cascade control structure includes two loops which are coupled to each other. The loops (speed loop and flux loop) consists of the Proportional-Integral Controller (PI-Controller) and the current Feedforward block while the inner loop (current loop) contains another PI block combined with a voltage Feedforward block. Here, the current controller for the current loop is first designed to guarantee that $i_{sd} \rightarrow i_{sd}*$, $i_{sq} \rightarrow i_{sq}*$ sufficiently fast with respect to the variations of the desired trajectories $\omega \rightarrow \omega*$ which will be achieved by the mechanical subsystem (speed loop). Then, a speed controller is synthesized and it should be noted that these two PI controller blocks are used to compensate the currents and speed static errors.

3.2.1 Speed reference trajectory design

Speed loop is designed based on motion and momentum equations of asynchronous motor as follows

$$J\frac{d\omega}{dt} = \frac{3}{2}z_p(1-\sigma)L_s\psi'_{rd}i_{sq} - m_W \quad (11)$$

Thus, we switch equation (11) to discrete-time domain obtained equation (12)

$$J\frac{1}{2T}[3\omega(k) - 4\omega(k-1) + \omega(k-2)] = \frac{3}{2}z_p(1-\sigma)L_s\psi'_{rd}(k)i_{sq}(k) - m_W \quad (12)$$

Based on the principle of flatness systems for the speed loop, we calculate the feedforward components

$$i^*_{sq-ff}(k) = \frac{J\frac{1}{2T}[3\omega^*(k) - 4\omega^*(k-1) + \omega^*(k-2)] + m_W}{\frac{3}{2}z_p(1-\sigma)\psi'^*_{rd}(k)} \quad (13)$$

To eliminate the deviation, we need to add a feedback regulator:

$$i^*_{sq-fb}(k) = i^*_{sq-fb}(k-1) + r_{0\omega}[\omega^*(k) - \omega(k)+r01\omega*k-1-\omega(k-1) \quad (14)$$

Then

$$i^*_{sq}(k) = i^*_{sq-ff}(k) + i^*_{sq-fb}(k) \quad (15)$$

$$i^*_{sq-ff}(k) = \frac{J\frac{1}{2T}[3\omega^*(k) - 4\omega^*(k-1) + \omega^*(k-2)] + m_W}{\frac{3}{2}z_p(1-\sigma)\psi'^*_{rd}(k)} + i^*_{sq-fb}(k-1) + r_{0\omega}[\omega^*(k) - \omega(k)] + r_{01}[\omega^*(k-1) - \omega(k-1] \quad (16)$$

3.2.2 Flux controller design for current feedforward component

Similarly, we calculate the magnetic flux adjustment loop and then we have equation (17) from the mathematic model of Induction Motor.

$$3\psi'^*_{rd}(k) - 4\psi'^*_{rd}(k-1) + \psi'^*_{rd}(k-2) + \frac{1}{T_r}\psi'^*_{rd}(k) = \frac{1}{T_r}i^*_{sd-ff}(k) \quad (17)$$

Therefore, we have feedforward components as below

$$i^*_{sd-ff}(k) = T_r\left[3\psi'^*_{rd}(k) - 4\psi'^*_{rd}(k-1) + \psi'^*_{rd}(k-2) + \frac{1}{T_r}\psi'^*_{rd}(k)\right] \quad (18)$$

$$\begin{aligned} i^*_{sd}(k) = {} & T_r\left[3\psi'^*_{rd}(k) - 4\psi'^*_{rd}(k-1) + \psi'^*_{rd}(k-2) + \frac{1}{T_r}\psi'^*_{rd}(k)\right] + i^*_{sd-fb}(k-1) \\ & + r_{0\omega}[\psi'^*_{rd}(k) - \psi'_{rd}(k)] \\ & + r_{01}[\psi'^*_{rd}(k-1) - \psi'_{rd}(k-1)] \end{aligned} \quad (19)$$

3.2.3 Voltage feedforward component

From the proposed current model (10), we have feedforward components as shown in (20)

$$\begin{cases} u_{sd-ff}(k) = \frac{1}{aT}\begin{bmatrix} i^*_{sd}(k+1) \\ -(1-dT)i^*_{sd}(k) \\ -\omega_s(k)Ti^*_{sq}(k) \\ -cT\psi'_{rd}(k) \end{bmatrix} \\ u_{sq-ff}(k) = \frac{1}{aT}\begin{bmatrix} i^*_{sq}(k+1) \\ -(1-dT)i^*_{sq}(k) \\ +\omega_s(k)Ti^*_{sd}(k) \\ +cT_r\omega^*(k)T\psi'^*_{rd}(k) \end{bmatrix} \end{cases} \quad (20)$$

Therefore, we have feedback components

$$\begin{cases} u_{sd-fb}(k) = u_{sd-fb}(k-1) \\ \quad +r_{0i}[i^*_{sd}(k) - i_{sd}(k) +] \\ \quad +r_{1i}[i^*_{sd}(k-1) - i_{sd}(k-1)] \\ u_{sq-fb}(k) = u_{sq-fb}(k-1) \\ \quad +r_{0i}[i^*_{sq}(k) - i_{sq}(k) +] \\ \quad +r_{1i}[i^*_{sq}(k-1) - i_{sq}(k-1)] \end{cases} \quad (21)$$

Thus, we have the control signals for induction motor as shown in (22)

$$\begin{aligned} u_{sd}(k) &= u_{sd-ff}(k) + u_{sd-fb}(k) \\ u_{sq}(k) &= u_{sq-ff}(k) + u_{sq-fb}(k) \end{aligned} \quad (22)$$

4. Simulation results

The parameters of Induction Motor using in simulation and experiment are shown in Table 1.

Table 1 IM parameters for simulation and experiment

Parameters	Value	Unit
Nominal power, P_N	0.18	kW
Nominal current I_N	1.0	A
Nominal frequency, f_N	60	Hz
Number of poles, z_p	2	Pole pairs
Nominal speed, n_N	1800	rpm
Nominal voltage, U_N	220	V
Stator resistance, R_s	11.05	Ω
Rotor resistance, R_r	6.11	Ω
Stator inductance, L_s	0.316423	H
Rotor inductance, L_r	0.316423	H
Mutual inductance, Lm	0.293939	H

4.1 Case 1: When grow speed from 53.61 rad/s up 107.22 rad/s and without load in time 1 s

Trajectory the reference speed: At the moment t = 0.03s the motor starts up at 53.61 rad/s, at t = 0.3 s the motor accelerates to 107.22 rad/s and stays the same until the time t = 0.7 s is reduced to 53.61 rad/s.

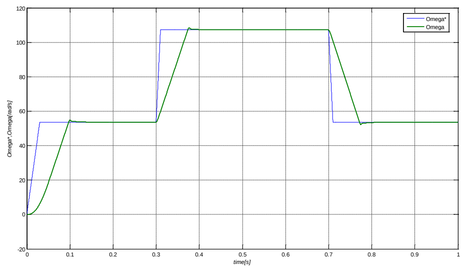

Figure 3 Response speed

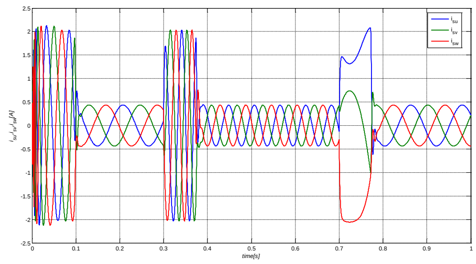

Figure 4 Response three-phase currents

At the start of startup, the actual speed at which the speed is set at 0.1 s is after the time interval 0.07 s. After a period of 0.08 s, the motor accelerated from 53.61 rad/s to 107.22 rad/s.

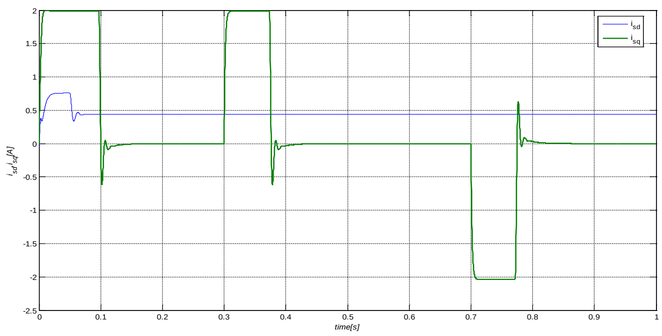

Figure 5 The components i_{sd} and i_{sq}

At the time of magnetization, the maximum i_{sd} 0.67 A, when the motor starts up, the i_{sd} current component is constant and equals the rated value of 0.45 A. At startup time, the i_{sq} component is the largest at 2.01 A. When booting successfully, the i_{sq} component is reduced to 0.

4.2 Case 2: When accelerating from 53.61 rad/s to 107.22 rad/s over a 2 seconds period and without load

Trajectory the reference speed: At t = 0.03 s, the motor starts up at 53.61 rad/s, at t = 0.6 seconds the motor accelerates to 107.22 rad/s and stays the same until the time t = 1.4 s is reduced to 53.61 rad/s.

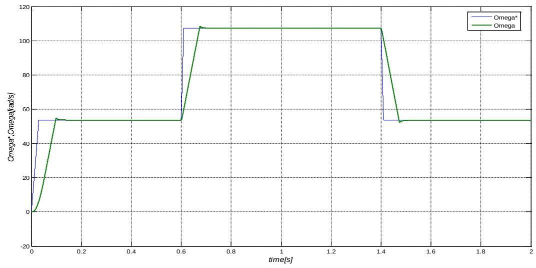

Figure 6 Response speed

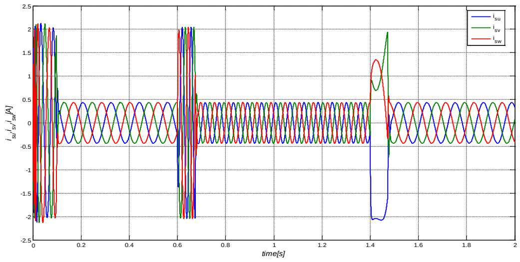

Figure 7 Response three-phase currents

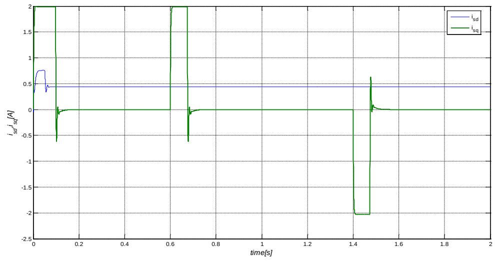

Figure 8 The components i_{sd} and i_{sq}

4.3. Case 3: When reversing from 53.61 rad/s to -53.61 rad/s for 2 seconds and not loading

Trajectory the reference speed: At the moment t = 0.03 s the motor starts up at a speed of 53.61 rad/s, at t = 0.6 s the motor reverses to a speed of -53.61 rad/s and is kept until the time t = 1.4s, it reverses the speed of 53.61 rad/s.

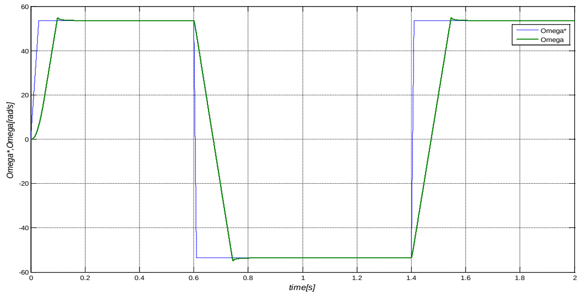

Figure 9 Response speed

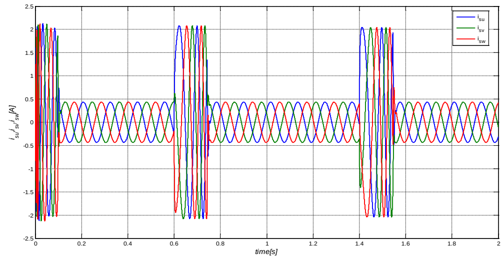

Figure 10 Response three-phase currents

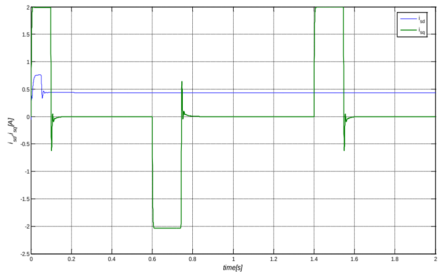

Figure 11 The components i_{sd} and i_{sq}

4.4. Case 4: When accelerating from 94.25 rad/s to 188.5 rad/s for 1 second and without load

Trajectory the reference speed: At the moment t = 0.03 s the motor starts up at a speed of 94.25 rad/s, at t = 0.3 seconds the motor accelerates to 188.5 rad/s and stays the same. By the time t = 0.7 s, the deceleration was 94.25 rad/s.

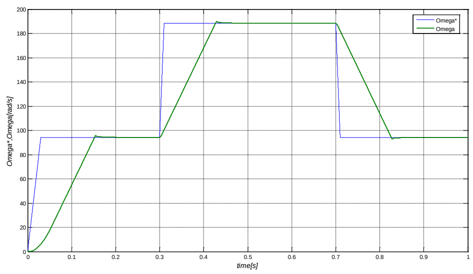

Figure 12 Response speed

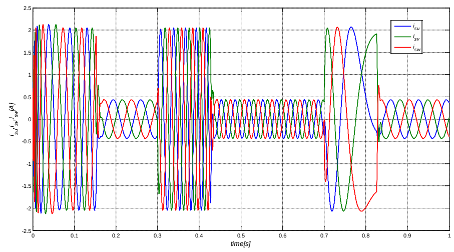

Figure 13 Response three-phase currents

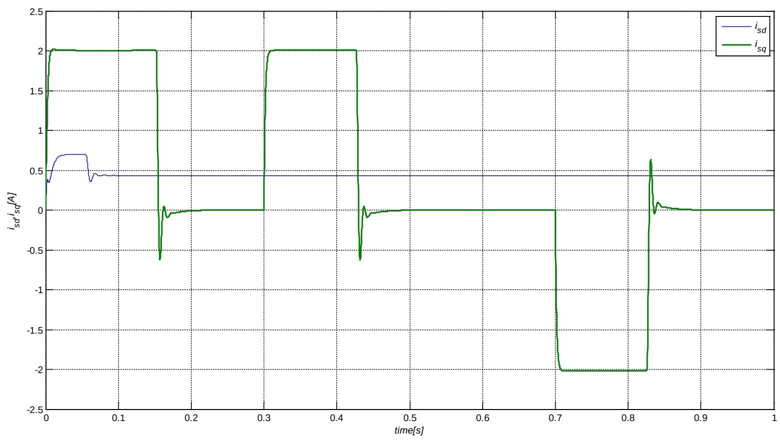

Figure 14 The components i_{sd} and i_{sq}

4.5 Case 5: When reversing from 94.25 rad/s to -94.25 rad/s for 1 second and not loading

Trajectory the reference speed: At the moment t = 0.03 s the motor starts up at a speed of 94.25 rad/s, at t = 0.3 s the motor reverses to -94.25 rad/s and is kept until the time t = 0.7 s, reversing the speed of 94.25 rad/s.

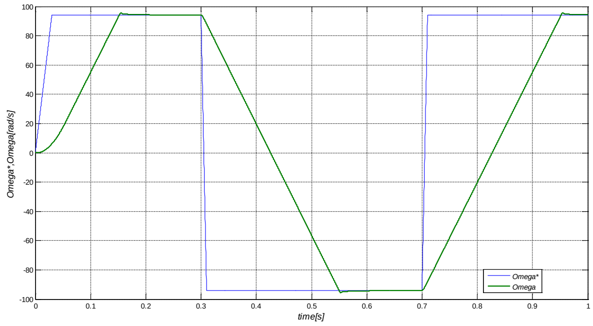

Figure 15 Response speed

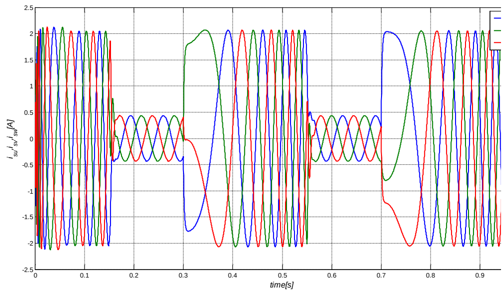

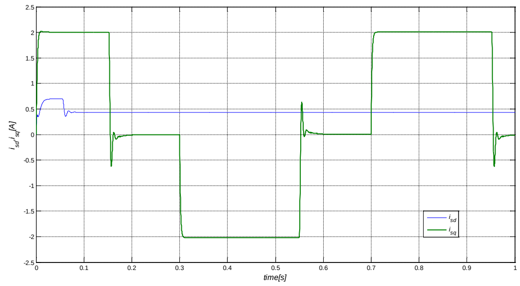

Figure 16 Response three-phase currents

Figure 17 The components i_{sd} and i_{sq}

4.6. Case 6: When accelerating from 94.25 rad/s to 188.5 rad/s and closing the load at 0.5 *s*

Some features gained during the simulation.

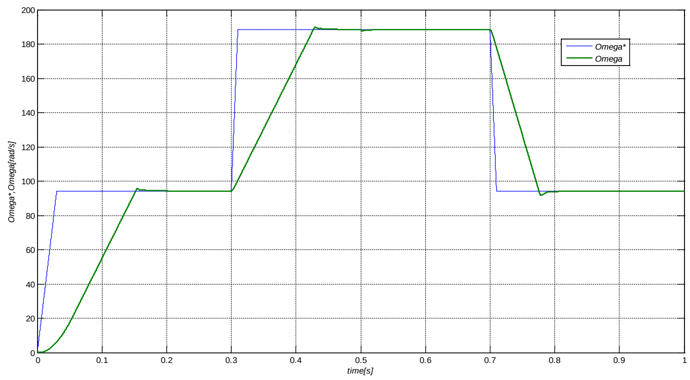

Figure 18 Speed responses of IM

At the start of startup, the actual speed at which the speed is set at 0.16 s is after 0.13 s. After 0.12 s, the motor accelerates from 94.25 rad/s to 188.5 rad/s.

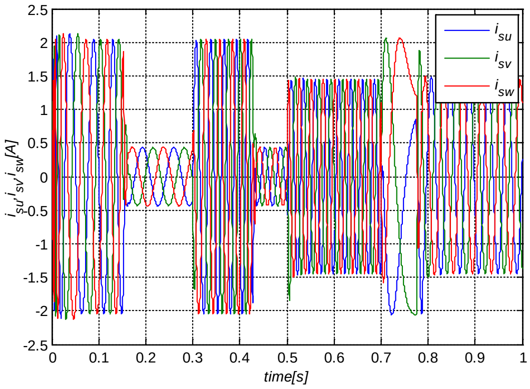

Figure 19 Response three-phase currents

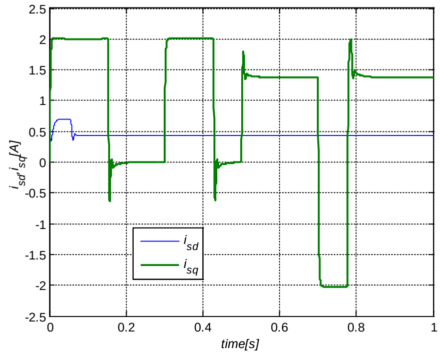

Figure 20 The components i_{sd} and i_{sq}

At the time of magnetization, the maximum i_{sd} 0.67 A, when the motor starts up, the i_{sd} current is constant and equal to the rated value of 0.45 A. At startup the i_{sq} component is the largest at 2.01 A. On successful startup, the i_{sq} component is reduced to 0. When the 100% load is closed at 0.5 s the i_{sq} current is equal to the rated current of 1.34 A.

5. Experimental results and discussion

5.1 Experimental system

The experimental structure consists of as follows:

- Experimental motors: The motors are asynchronous crankshaft rotor; the motor speed is measured by the encoder attached to the motor.
- Load for engine.
- Experimental inverters: Experimental inverters include power valves, DSPs TMS320F28335 for control programs, current measurement circuits, DC voltage measurement circuits, coupling circuits to encoder for feeding back degree of motor.
- Measuring devices: oscilloscopes, multimeters, ampere pliers, and computer.
- Three-phase self-transformer.

In this experimental system, the structure of the experimental inverter, as shown in Figures 21 and 22, consists of the following modules: Capacity module, measurement module, control module, and additional functions.

The experimental system consists of: Experimental drives (power circuits and measurement, protection and control), motors, loads, measuring instruments including: multimeter, oscilloscope. Experimental design and construction are structurally and functionally similar to commercial inverters but are very flexible allowing direct interference with software and installing control structures in the C programming language. The digital signal processor used here is DSP TMS320F28335.

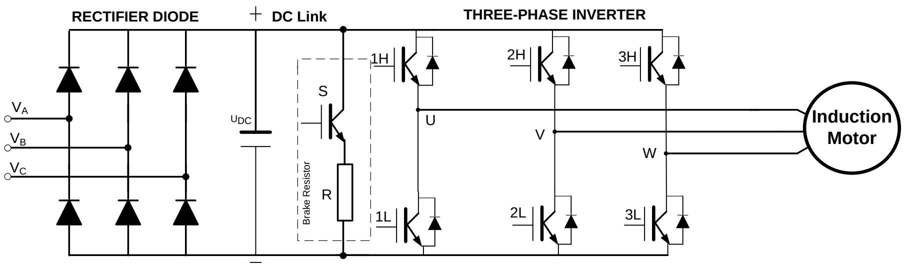

Figure 21 Power circuit structure of the experimental inverter

JCST Vol.10 No.2 Jul.-Dec. 2020, pp. 165-181
ISSN 2630-0656 (Online)

Figure 22 Detailed depiction of experimental inverter

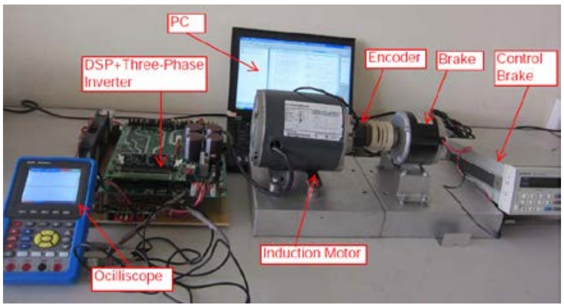

Figure 23 Experimental system

5.2 Experimental results

5.2.1 Case 1: When accelerating the motor from 53.61 rad/s to 107.22 rad/s for 1 second

Trajectory the reference speed: At t = 0.03 s the motor starts at 53.61 rad/s, at t = 0.3 s the motor accelerates to 107.22 rad/s and stays the same until at t = 0.7 s, deceleration is 53.61 rad/s. Start-up, acceleration and deceleration are performed in 1 second (Figure 24a).

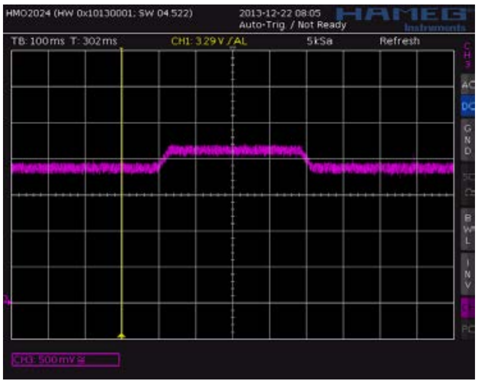

a) Reference speed

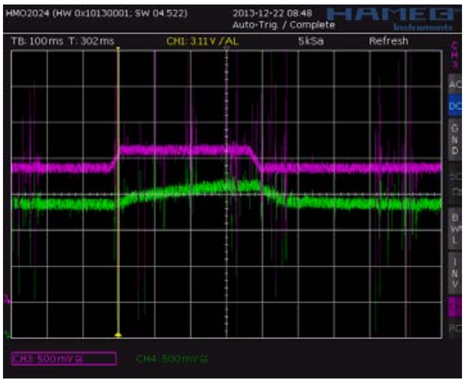

b) Reference and actual speed of the motor

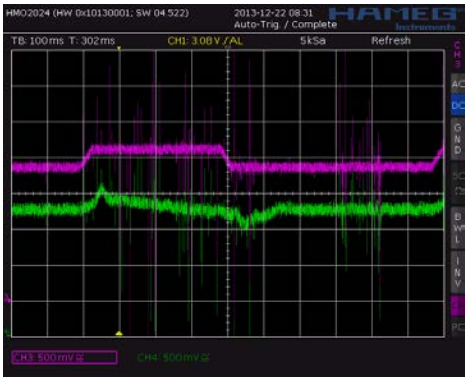

c) Reference speed and i_{sd} current when no load

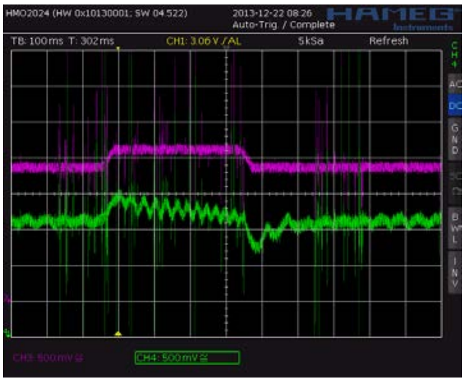

d) Reference speed and i_{sq} current when no load

Figure 24 Speed and dq components stator current of the motor when accelerating the motor

5.2.2. Case 2: When accelerating the motor from 53.61 rad/s to 107.22 rad/s for 2 seconds

Trajectory the reference speed: At the moment t = 0.03 s the motor starts up at 53.61 rad/s, at t = 0.6 seconds the motor accelerates to 107.22 rad/s and stays the same until at t = 1.4 s, deceleration is 53.61 rad/s. Startup, acceleration and deceleration are performed in 2 seconds.

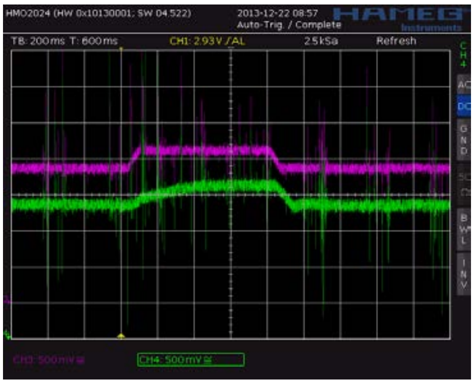

a) Reference speed and actual speed

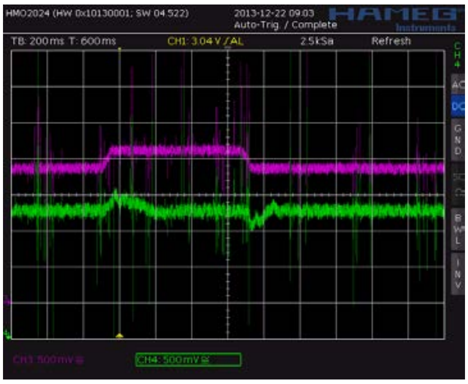

b) Reference speed and i_{sd} current when no load

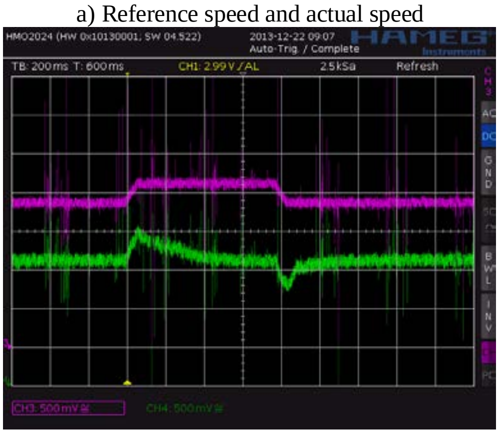

c) Reference speed and i_{sq} current when no load

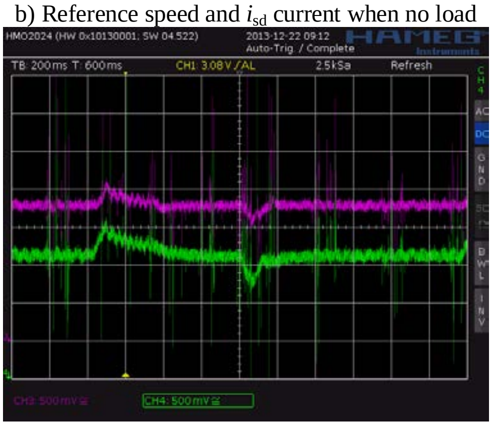

d) i_{sd} current (above) and i_{sq} current (bottom)

Figure 25 Speed and dq components stator current of the motor when accelerating the motor

5.2.3. Case 3: When reversing from 53.61 rad/s to -53.61 rad/s over 2 seconds

Trajectory the reference speed: At the moment t = 0.03 s, the motor starts up at 53.61 rad/s, at time t = 0.4 s the motor reverses to -53.61 rad/s and is held until the time t = 1.4 s, it reverses the speed of 53.61 rad/s. The process of starting, reversing 2 times is done in 2 seconds.

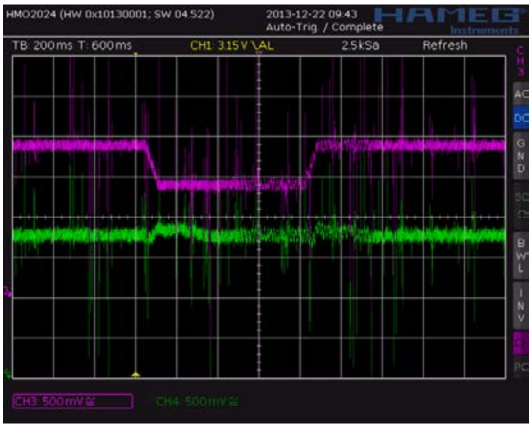

a) Reference speed and i_{sd} current

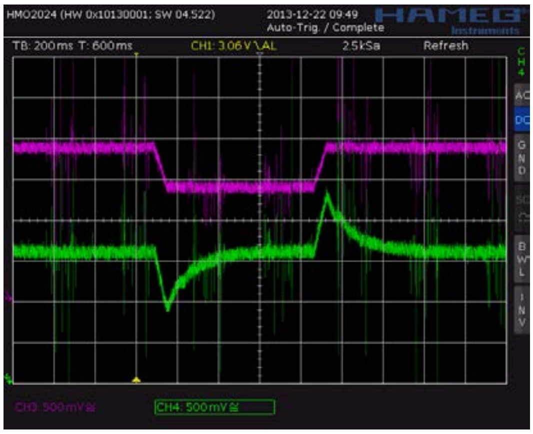

b) Reference speed and i_{sq} current

JCST Vol.10 No.2 Jul.-Dec. 2020, pp. 165-181
ISSN 2630-0656 (Online)

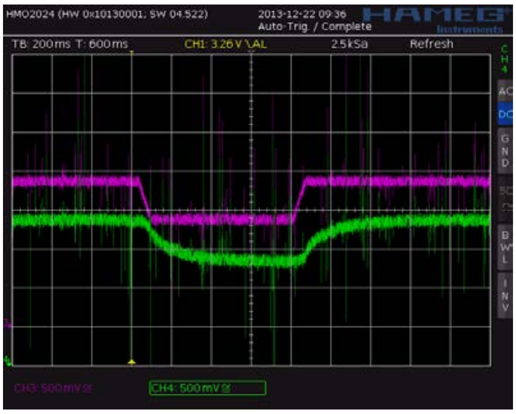

c) Reference speed and actual speed

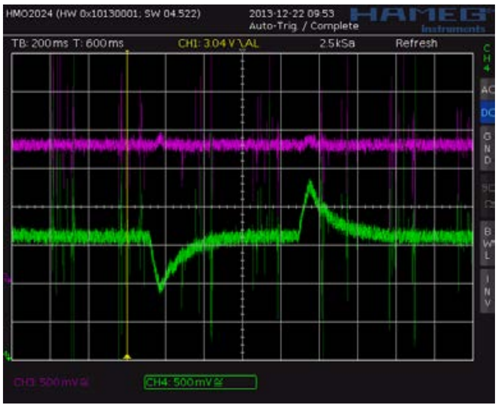

d) i_{sd} current (above) and i_{sq} current (bottom)

Figure 26 Speed and dq components stator current of the motor when reversing

At the moment the acceleration i_{sq} is increased to 3.6 A. From the empirical results of the i_{sd}, i_{sq} in both accelerated and reversed cases show the channel separation characteristic between the two stream components.

5.2.4. Case 4: When accelerating the motor from 94.25 rad/s (900 rpm) to 188.5 rad/s (1800 rpm) for 1 second

Speed reference trajectory: At the moment t = 0.03 s, the IM starts in 94.25 rad/s speed at t = 0.3 s, the speed of motor accelerates to 188.5 rad/s and stays the same speed until t = 0.7 s, then the deceleration speed is 94.25 rad/s. Startup, acceleration and deceleration are performed in 1s, this result is considered as a good state of startup process.

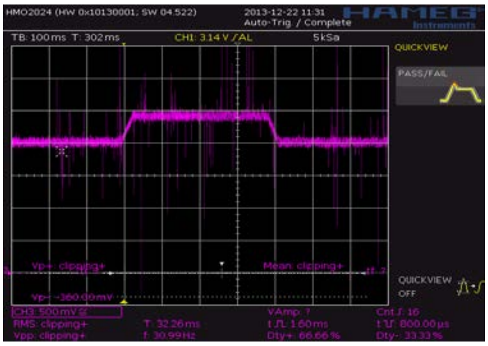

a) Reference speed

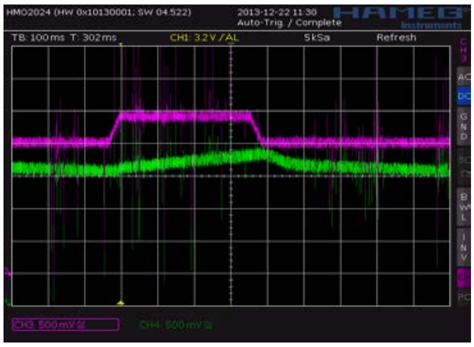

b) Reference speed and actual speed

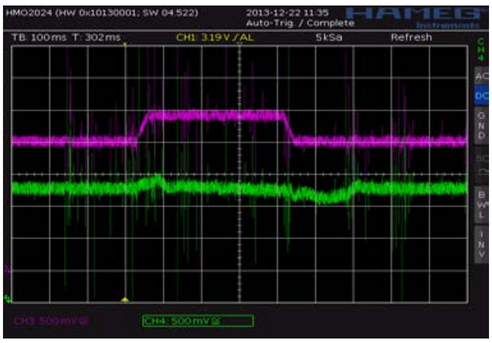

c) Reference speed and i_{sd} current

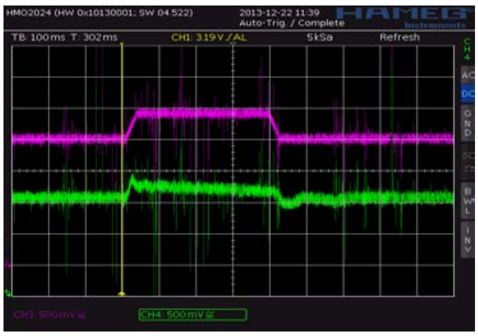

d) Reference speed and i_{sq} current

Figure 27 Speed and dq components stator current of the motor when accelerating the motor

The i_{sd} and i_{sq} components current increased to 2.1 A at the time of acceleration. We find that the real speed is very close to the set speed.

5.2.5 Case 5: When reversing from 94.25 rad/s (900 rpm) to -94.25 rad/s for 1 second

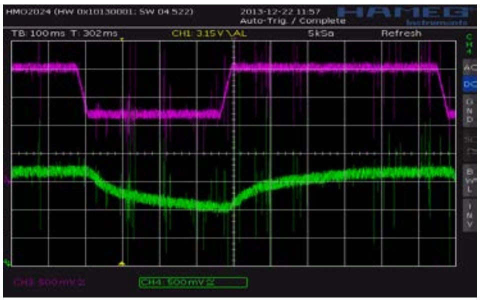

a) Reference speed and actual speed

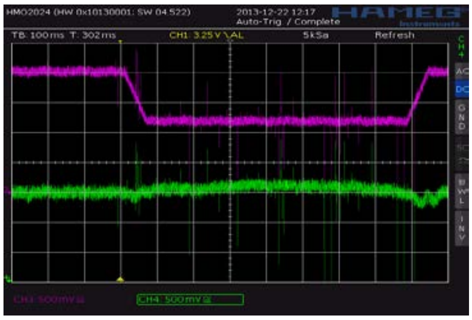

b) Reference speed and i_{sd} current

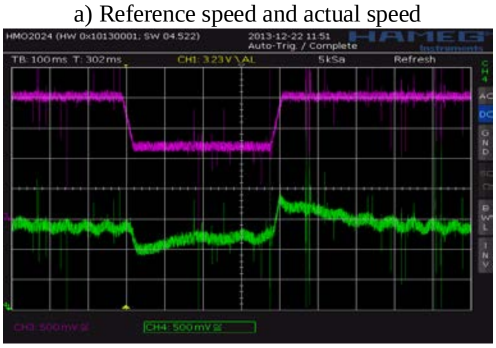

c) Reference speed and i_{sq} current

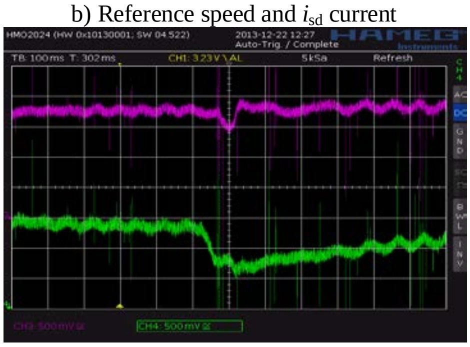

d) i_{sd} current (above) and i_{sq} current (bottom)

Figure 28 Speed and dq components stator current of the motor when reversing

Trajectory the reference speed: At the moment t = 0.03 s, the motor starts up at 94.25 rad/s, at t = 0.3 s the motor reverses to -94.25rad s and is held until the time t = 0.7s, the speed back to 94.25 rad/s. Start-up, reversal is performed in 1 second.

5.2.6. Case 6: When the motor is operating at a rated speed of 188.5 rad/s (1800 rpm) with load

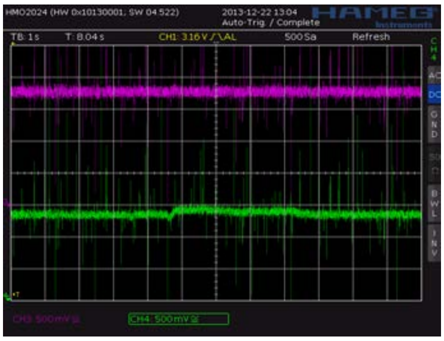

a) i_{sd}, i_{sq} current components when 50% load

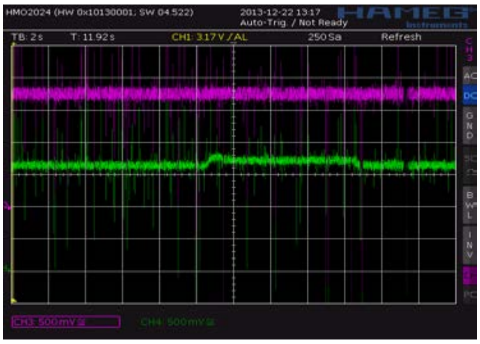

b) i_{sd}, i_{sq} current components when 70% load

Figure 29 Characteristics when imposing load

When the load is constant, the i_{sd} current component is constant, the i_{sq} current component increases with the load. When the load is 70% of the i_{sq} current around 1 Ampere, it can be seen that the empirical results reflect the desired perceptions correctly. The load changing is the main factor which is caused by nonlinearity of the IM, and experimental results are shown that the proposed CFBC strategy reduced the effect of nonlinear problem in both startup and load changing process of IM.

6. Conclusions

In this paper, we review the nonlinear problem of IM discrete-time control. The motivations are to eliminate the static errors of state variables and to solve the nonlinear characteristics of IM control system by using the proposed SFBC scheme. In which, through Taylor series expansion and differential flatness, three controllers of the current, speed and flux loops are used to eliminate the static errors. Then, 6 cases of simulation are shown to demonstrate the effectiveness of the proposed CFBC. The performance evaluation is given by experimental results. For example, when the load and i_{sd} current component are constant, the i_{sq} current component increased with the load. Meanwhile the load is 70% of the i_{sq} current about 1 Ampere, it can be seen that the empirical results reflect the desired perceptions correctly. Finally, we conclude the proposed CFBC can improve the effectiveness of IM with high speed and accuracy even if the nonlinear characteristics of the IM are taken into account in the process of control.

7. References

Beaty, H. W., & Kirtley, J. L. (1998). *Electric motor handbook.* New York, USA: McGraw-Hill.

Broocker, M., & Lemmen, M. (2001). Nonlinear control methods for disturbance rejection on a hydraulically driven flexible robot. In *Proceedings of the Second International Workshop on Robot Motion and Control. RoMoCo'01 (IEEE Cat. No.01EX535), Bukowy Dworek, Poland, 2001*, pp. 213-218. DOI: 10.1109/ROMOCO.2001.973457

Dang, X. K., Ho, L. A. H., Do, V.-D. (2018). Analyzing the sea weather effects to the ship maneuvering in Vietnam's Sea from BinhThuan province to Ca Mau province based on fuzzy control method. *TELKOMNIKA Telecommunication, Computing, Electronics and Control, 16*(2), 533-543. DOI: http://dx.doi.org/10.12928/telkomnika.v16i2.7753

Dang, X., Guan, Z., Tran, H., & Li, T. (2011). Fuzzy adaptive control of networked control system with unknown time-delay. In *Proceedings of the 30th Chinese Control Conference*, Yantai, China, pp. 22-24.

Dannehl, J., & Fuchs, F., W. (2006). Flatness-based control of an induction machine fed via voltage source inverter - concept, control design and performance analysis. *IECON 2006 - 32nd Annual Conference on IEEE Industrial Electronics*, 5125-5130. DOI: 10.1109/IECON.2006.347840

Delaleau, E. & Stankovic, A. M. (2004). Flatness-based hierarchical control of the PM synchronous. *Proceedings of the 2004 American Control Conference, Boston, MA, USA, 2004, vol.1,* 65-70. DOI:10.23919/acc.2004.1383580

Do, V.-D., & Dang, X. K. (2018). Optimal control for dynamic positioning system based on fuzzy-PSO advanced technical. *TELKOMNIKA (Telecommunication, Computing, Electronics and Control)* Vol.16, No.6, pp. 2999-3007. DOI: 10.12928/TELKOMNIKA.v16i6.8979

Do, V.-D., & Dang, X. K. (2019). The fuzzy particle swarm optimization algorithm design for dynamic positioning system under unexpected impacts. *Journal of Mechanical Engineering and Sciences (JMES), 13*(3), 5407-5423. DOI: https://doi.org/10.15282/jmes.13.3.2019.13.0439

Fan, L., & Zhang, L. (2011a). Fuzzy based flatness control of an induction motor. *Procedia Engineering, 23,* 72-76. DOI: https://doi.org/10.1016/j.proeng.2011.11.2467

Fan. L., & Liang. Z. (2011b). An improved vector control of an induction motor based on flatness. *Procedia Engineering, 15*(November), 624-628. DOI: http://dx.doi.org/10.1016/j.proeng.2011.08.116

Faustner, D., Kemmetmuller, W., & Kugi, A. (2015). Field weakening in flatness-based torque control of saturated surface-mounted permanent magnet synchronous machines. *In 2015 IEEE Conference on Control Applications (CCA)*, Sydney, NSW, 2015, pp. 858-863. DOI: 10.1109/CCA.2015.7320725

Faustner, D., Kemmetmüller, W., & Kugi, A. (2016). Experimental parameterization of a design model for flatness-based torque control of a saturated surface-mounted PMSM. *IFAC-PapersOnLine*, 49(21): 575-582. DOI: http://dx.doi.org/10.1016/j.ifacol.2016.10.663

Fliess, M., & Marquez, R. (2000). Continuous-time linear predictive control and flatness: A module-theoretic setting with examples. *International Journal of Control*, *73*(7), 606-623. DOI: https://doi.org/10.1080/002071700219452

Fliess, M., Lévine, J., Martin, P., & Rouchon, P. (1992). On differentially flat nonlinear systems. *IFAC Proceedings*, *25*(13), 159-163. DOI: https://doi.org/10.1016/S1474-6670(17)52275-2

Fliess, M., Lévine, J., Martin, P., & Rouchon, P. (1999). A Lie-Bäcklund approach to equivalence and flatness of nonlinear systems. In *IEEE Transactions on Automatic Control*, *44*(5), 922-937. DOI: 10.1109/9.763209

Graichen, K., Hagenmeyer, V., & Zeitz, M. (2006). Feedforward control with online parameter estimation applied to the Chylla-Haase reactor benchmark. *Journal of Process Control*, *16*, 733-745. DOI: 10.1016/j.jprocont.2006.01.001

Hagenmeyer, V., & Delaleau, E. (2003). Exact feedforward linearization based on differential flatness. *International Journal of Control*, *76*(6), 537-556. DOI: https://doi.org/10.1080/0020717031000089570

Hagenmeyer, V., & Delaleau, E. (2004). A robustness analysis with respect to exogenous perturbations for flatness-based exact feedforward linearization. *IFAC Proceedings Volumes*, *37*(13), 195-200. DOI: https://doi.org/10.1016/S1474-6670(17)31222-3

Hagenmeyer, V., & Delaleau, E. (2008). Continuous-time non-linear flatness-based predictive control: An exact feedforward linearisation setting with an induction drive example. *International Journal of Control*, *81*(10), 1645-1663. DOI: https://doi.org/10.1080/00207170802090177

Hagenmeyer, V., & Delaleau, E. (2010). Robustness analysis with respect to exogenous perturbations for flatness-based exact feedforward linearization. In *IEEE Transactions on Automatic Control*, 55(3), 727-731. DOI: 0.1109/TAC.2010.2040425

Henke, B., Rue, A., Neumann, R., Zeitz, M., & Sawodny, O. (2014). Flatness-based MIMO control of hybrid stepper motors - design and implementation. In *2014 American Control Conference, Portland, OR, 2014*, pp. 347-352. DOI: 10.1109/ACC.2014.6858602

Houari, A., Renaudineau, H., Martin, J.-P., Pierfederici, S., & Meibody-Tabar, F. (2012). Flatness-based control of three-phase inverter with output LC filter. In *IEEE Transactions on Industrial Electronics*, *59*(7), 2890-2897. DOI: 10.1109/TIE.2011.2170396

Levine, J. (2009). *Analysis and control of nonlinear system: A flatness-based approach.* Springer (c). ISBN: 978-3-642-00838-2. https://www.springer.com/gp/book/9783642008382

Maaziz, M., Siguerdidjane, H., Boucher, P., & Dumur, D. (1999). Nonlinear predictive control of current-fed induction motor based on differential flatness properties. In *Proceedings 5th European Control Conference (ECC)*, Karlsruhe, Germany, pp. 803-808. DOI: 10.23919/ECC.1999.7099404

Mahadevan, R., Agrawal, S., & Doyle, F. (2001). Differential flatness based nonlinear predictive control of fed-batch bioreactors. *Control Engineering Practice*, 9, 889-899. DOI: 10.1016/S0967-0661(01)00054-5

Noda, Y., Zeitz, M., Sawodny, O., & Terashima, K. (2011). Flow rate control based on differential flatness in automatic pouring robot. In *Proceedings of IEEE International Conference on Control Applications (CCA).* Denver, CO, USA. DOI: 10.1109/CCA.2011.6044508

Sira-Ramirez, H. (2000). A passivity plus flatnedd controller for the permanent magnet stepper motor. *Asian Journal of Control, 2*(1), 1 – 9. DOI: 10.1111/j.1934-6093.2000.tb00139.x

Thanh, P. T., & Quang, N. P. (2013). Quasi-Continuous Implementation of Structural Nonlinear Controller Based on Direct-Decoupling for Permanent Magnet Synchronous Motor. *IEEE International Conference on Control, Automation and Information Sciences, Nha Trang, Vietnam*, 283-288. DOI: 10.1109/ICCAIS.2013.6720569

Thomsen, S., & Fuchs, F. W. (2010). Flatness based speed control of drive systems with resonant loads. *IECON 2010 - 36th Annual Conference on IEEE Industrial Electronics Society*, Glendale, AZ, 2010, pp. 120-125. DOI: 10.1109/IECON.2010.5675188

Wang, X., Zhong, H., Yang, Y., & Mu, X. (2010). Study of a novel energy efficient single-phase induction motor with three series-connected windings and two capacitors. *IEEE Transactions on Energy Conversion, 25*(2), 433-440. DOI: 10.1109/TEC.2009.2039218